Cellulose (2024) 31:349–361
https://doi.org/10.1007/s10570-023-05621-x

ORIGINAL RESEARCH

Bacterial cellulose nanofibrous aerogels grafted with citric acid for absorption and separation of protein

Jianwei Lu · Yangang Jiang · Zihao Wen · Zhengjin Luo · Yufei Qiao · Li Guo

Received: 8 June 2023 / Accepted: 14 November 2023 / Published online: 29 November 2023

Abstract The design and construction of high-performance protein absorbents are of great significance for obtaining highly purified proteins in the field of biotechnology and more. In this study, the highly carboxylated absorption media were fabricated for selective absorption of positively charged proteins by using bacterial cellulose (BC) nanofibrous aerogel (NFA) as a substrate material in concert with citric acid (CA). The obtained BC/CA NFAs exhibited highly interconnected open porous structure, surface hydrophilicity, large specific surface area (14.2 m^2/g), good elasticity and compression fatigue resistance. BC/CA NFAs displayed a high lysozyme absorption capacity of 868.9 mg/g and fast equilibrium within 2.5 h. A dynamic lysozyme absorption capacity of 655.35 mg/g was achieved under the drive of gravity, meeting the demands of actual applications. Furthermore, BC/CA NFAs exhibited unique absorption selectivity performance, good reusability, as well as acid and alkaline resistance. A successful scale-up of such environmental friendliness, low cost and good reproducibility absorbents could provide a new perspective to develop next generation three-dimensional chromatographic media for substantial bio-separation applications.

Graphical abstract

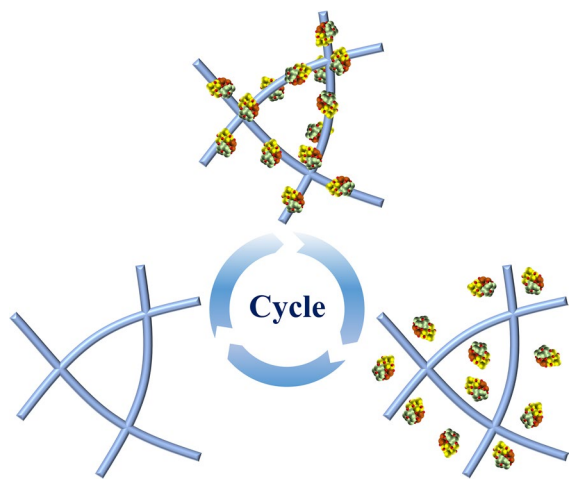

Keywords Bacterial cellulose · Nanofibrous aerogel · Large specific surface area · Protein absorption performance · Environmental friendliness

Supplementary Information The online version contains supplementary material available at https://doi.org/10.1007/s10570-023-05621-x.

J. Lu (✉) · Y. Jiang · Z. Wen · Z. Luo · Y. Qiao · L. Guo (✉)
School of Materials Science and Engineering, Jiangsu University, Zhenjiang 212013, China
e-mail: jianwei@ujs.edu.cn

L. Guo
e-mail: liguo@ujs.edu.cn

Introduction

Protein purification is an important bio-separation technology in the fields of biochemistry, which has been applied in immunotherapy, pharmaceutical, food engineering and health care (Zhao et al. 2022; Ebrahimi et al. 2023; Fang et al. 2022; Zhang et al. 2023). To date, several protein purification techniques mainly including sedimentation, centrifugation, electrophoresis, precipitation, absorption and separation, have been developed to obtain highly purified proteins (Ogata et al. 2022; Kluszczynska et al. 2022; Arbita et al. 2022). Among them, absorption and separation are the most widely applied strategies owing to their high accuracy and good universality (Ge et al. 2019; Yi et al. 2017). The protein absorption and separation process are carried out by porous resin or micro-nano spheres packed chromatography columns. However, these packed media are generally subjected the drawbacks of large pressure drops, long retention time and low flow rates, limiting the further development in large-scale protein purification (Jain et al. 2007; Ghosh 2002). Fortunately, fibrous-based protein absorption media with favorable features of surface transmission and absorption have proved to be potential materials for solving the shortcomings of the packed porous resin or micro-nano spheres (Wang et al. 2020; He et al. 2015). Nonetheless, those fibrous-based media usually exhibit relatively low absorption capacity, which is caused by their relatively insufficient absorption ligands, comparatively large fiber diameters and small specific surface area (Orr et al. 2013).

Nanofibers, well-known materials having favorable features of large specific surface area, high porosity and ease of surface functionalization, have become promising building blocks for fabricating media with good absorption performance (Dou et al. 2019; Fu et al. 2018). Yi (Yi et al. 2018) et al. grafted sulfated groups on the surface of silk fibroin nanofibrous membranes (NFMs) under mild conditions for the absorption of *Candida rugosa* lipase (148.0 mg/g). Li (Li et al. 2017) et al. functionalized polyacrylonitrile (PAN) NFMs with lysine (LYS) to obtain pH-controllable PAN-LYS NFMs, resultant NFMs exhibited good absorption performance on pepsin (425.5 mg/g) and lysozyme (55.0 mg/g). Rajesh (Rajesh et al. 2018) et al. fabricated cellulose-graft-polyethyleneamidoamine anion-exchange NFMs by using redox polymerization with a bovine serum albumin capturing capacity of 239.0 mg/g. Despite the absorption performance of NFM-based media has been improved at a certain degree, the two-dimensional (2D) NFMs still face pivotal bottlenecks of relatively low absorption capacity and slow biomolecules transmission, which were caused by the 2D structure of NFMs' intrinsic limitations (Yi et al. 2017). Besides, the 2D thin membranes could hardly be assembled into large-sized chromatography columns (Przybycien et al. 2004).

Compared with 2D nanofibrous membrane structure, three-dimensional (3D) nanofibrous aerogel (NFA) structure possesses a larger specific surface area, higher porosity, controllable physicochemical properties and adjustable shape, which render 3D aerogels be a promising candidate for constructing high-performance protein absorption media (Cheng et al. 2022). Recently, several aerogels based on electrospun nanofibers was prepared for protein absorption, resulting in the steep improvement of protein absorption capacity (Fu et al. 2019a, 2019b). However, the fabrication of electrospun NFA absorbents still face the issues of high cost, poor biocompatibility and degradability, residues and volatilization of organic solvent, uncontrollable and inhomogeneous structures (Yu and Sun 2013; Dou et al. 2019), which is hard to meet global sustainable development trend.

Natural polysaccharides, especially bacterial cellulose (BC), are deemed as promising components for protein absorption, resulting from their inherent properties of good biocompatibility and hydrophilicity (Sharma et al. 2017, 2019, 2020; Chen et al. 2019; Zhan et al. 2019). BC, as a low cost and renewable green biomass material, has been successfully prepared into 3D aerogels, which possess the characteristic of both 3D aerogel structure and BC (Leitch et al. 2016; Hu et al. 2023). Moreover, the abundant active hydroxyl groups on the surface of cellulose can be used for subsequent modification under very mild methods to enhance application adaptability (Beaumont et al. 2016, 2021a, b; Das et al. 2022). The porous network structure of BC NFAs can effectively bind the protein molecules to the absorption ligands (Huang et al. 2022). As far as we know, seldom related research on protein absorbents based on BC were reported until now.

In this work, we demonstrated a simple, versatile and readily accessible strategy to design protein

absorbents based on BC nanofibers by combining freeze-drying and impregnation. BC nanofibers were selected as building blocks to construct NFA substrate through chemical cross-linking. Citric acid (CA) was grafted on BC NFAs to generate protein absorbents under the catalysis of polyphosphoric acid (PPA). The as-prepared BC/CA NFAs possessed highly interconnected open porous network, superhydrophilicity, large specific surface area, and robust mechanical strength. Benefiting from those fantastic structural properties, the BC/CA NFAs exhibited high absorption capacity, short absorption equilibrium time and good dynamic absorption property. Moreover, the selectivity, reversibility, acid and alkaline resistance of BC/CA NFAs were also systemically investigated.

Experimental section

Materials

Bacterial cellulose (BC) nanofiber sheets (diameter of 50.99 nm, Fig. S1) were obtained from Hainan Yeguo Foods Co., Ltd. Glutaraldehyde aqueous solution (50 wt%), acetic acid, polyphosphoric acid (PPA), citric acid (CA), phosphoric acid (H_3PO_4), sodium hydroxide (NaOH), phosphate buffer saline (PBS), lithium chloride (LiCl), magnesium chloride ($MgCl_2$), sodium chloride (NaCl) and potassium chloride (KCl) were all purchased from Sinopharm Chemical Reagent Co., Ltd. Lysozyme, bromelain, papain, ovalbumin, pepsin and bovine serum albumin were acquired from Sangon Biotech Co., Ltd. All commercial obtained chemical reagents were used without further purification or treatment.

Fabrication of BC nanofibrous aerogels (NFAs)

The BC NFAs were fabricated through freeze-drying and cross-linking process. Briefly, 0.1 g BC nanofibers were dispersed in 20 mL water through homogenizing for 20 min at 13,000 rpm (IKA T25 homogenizer) to form BC nanofibrous dispersions (0.5 wt%). The glutaraldehyde aqueous solution with a certain amount (100, 200, 300 and 400 μL) was then added into BC nanofibrous dispersions with mechanical stirring. The pH value of dispersions was adjusted to 3–4 by acetic acid solution. Subsequently, the obtained BC nanofibrous dispersions were freeze-dried to gain BC nanofibrous framework. Finally, BC NFAs were fabricated through heating in an air environment at 75 °C for 4 h.

Preparation of BC/CA NFAs

BC/CA NFAs were obtained through impregnation method. CA and PPA were chosen as modifying agent and catalyst, respectively. CA and PPA were dissolved into deionized water to form the modified solutions with various CA contents (0, 2, 4, 6, 8 and 10 wt%). BC NFAs were put into modified solutions with bath ratio 100/1 (w/w) for 30 min. The BC NFAs filled with modified solution were freeze-dried in a lyophilizer, and then were heated at 100 °C to undergo grafting polymerization to generate BC/CA NFAs with numerous absorption ligands.

Apparatus and characterization

The microstructure was observed by employing a scanning electron microscope (SEM, Hitachi U8230). The hierarchical porous structure and specific surface area were determined by using an ASAP 2020 analyzer (Micromeritics). The surface chemical bonds and composition were detected by using an attenuated total reflection-Fourier transform infrared spectrometer (ATR-FTIR, Nicolet 8700), X-ray photoelectron spectroscopy (XPS, Thermo Fisher K-alpha) and solid state Nuclear Magnetic Resonance spectrometer (13C NMR, JEOL-ECX400). The thermal properties were taken using a differential scanning calorimeter (PerkinElmer DSC4000) and thermogravimetric analyzer (TGA, TA instruments Q50). The surface wettability was measured by using a contact angle meter (Kino SL200B) with solution volume of 3 μL. The compression performances were characterized by using an Instron (model 5969) fitted with a 100 N load. The zeta potential was measured by using a Nano Zetasizer (ZS 90). The concentration of protein solutions was characterized by using an ultraviolet–visible (UV–Vis) spectrophotometer (UV-5200).

Protein absorption performance measurements

The PBS solutions were fabricated through adding PBS into deionized water with constantly stirring. The model proteins were dispersed in PBS solutions to obtain protein solutions with various pH values,

ionic strength, ion species and protein species. 20 mg BC/CA NFAs were immersed in 20 mL of protein solutions at room temperature, after a period of absorption, BC/CA NFAs were taken out and washed with PBS solutions to remove the non-specifically binding proteins and protein-fouling. The concentrations of protein solution were detected by using an ultraviolet–visible (UV–Vis) spectrophotometer. The protein absorption capacity of BC/CA NFAs were calculated by the following formula:

$$Q = \frac{(C_0 - C)V}{m} \quad (1)$$

where Q is the protein absorption capacity (mg/g), C_0 and C are the concentrations of protein solution before and after absorption (mg/mL), respectively, V is the volume of protein solutions (mL), m is the weight of BC/CA NFAs (mg).

Reusability measurements

The absorption-elution experiments were carried out for 10 cycles to evaluate the reusability of BC/CA NFAs. The absorbed BC/CA NFAs were treated in 2 M NaCl solution to elute the absorbed proteins. After that, the BC/CA NFAs were washed by deionized water to remove residual NaCl. The regenerated BC/CA NFAs were repeatedly immersed into protein solutions for several cyclic experiments.

Result and discussion

Design and fabrication of BC/CA NFAs

The protein absorption aerogels with high-performance should be designed and fabricated according to the following three criteria: (1) the surface wettability of resultant aerogels should exhibit good hydrophilicity to prevent nonspecific protein absorption; (2) the physicochemical structure of BC/CA CNFAs should be stable and robust to guarantee their long-term application; (3) abundant functional protein absorption ligands should be presented on aerogels to realize efficient absorption of proteins. The first criterion was satisfied by taking BC nanofibers with good hydrophilicity as building blocks. To satisfy the second criterion, glutaraldehyde was used as a cross-link agent, enhancing the mechanical properties of aerogels. The bonding among BC nanofibers observed in Fig. S2 was formed by cross-linking between glutaraldehyde and BC nanofibers. The last criterion was satisfied by choosing CA as a modifier and PPA as a catalyst, endowing the aerogels with rich absorption ligands (Fu et al. 2016).

As illustrated in Fig. 1a, the fabrication process of BC/CA NFAs mainly includes three steps: dispersion of BC nanofibers, formation of BC NFAs and carboxylic grafting. Firstly, dispersion was obtained through homogenizing BC nanofibers into water mixture solution. Subsequently, BC NFAs were formed via freeze-drying and cross-linking process, the BC nanofibers were well-distributed and bonded with each other (Lu et al. 2017). The BC NFAs were immersed into the modified solutions containing CA and PPA, then dried and heated to realize carboxylic grafting. The unreacted CA and PPA were removed by washing with deionized water to generate BC/CA NFAs. According to previous literature (Fu et al. 2016), the polymerization between BC and CA occurred at around 100 °C.

BC NFAs with good formability is the key for the synthesis of high-performance absorbent materials. The ether bonds (located at about 1054 cm^{-1}) formed by cross-linking process and residual aldehyde group (located at about 1712 cm^{-1}) on glutaraldehyde were detected by FTIR spectra (Fig. S3), indicating the successful cross-linking. The photograph of BC NFAs with various glutaraldehyde contents was displayed in Fig. S4. With increasing glutaraldehyde contents, the volume of BC NFAs decreased. When the glutaraldehyde content is high, BC NFAs deformed. While, BC NFAs with low glutaraldehyde contents collapsed in water (Fig. S5). This is due to that the weak bonds between BC nanofibers were destroyed by hydrogen bonds in the water (Zhang et al. 2012). Therefore, BC NFAs can maintain good stability in both air and water, when the content of glutaraldehyde is set at about 300 μL.

The process of carboxyl grafting on BC nanofibers is shown in Fig. 1b. CA with a large amount of carboxyl groups would be grafted onto nanofibers through esterification (Fu et al. 2019b). The changes in surface chemical compositions were determined by FTIR spectra analysis. As shown in Fig. 1c, compared with spectra of BC NFAs, the intensity of the characteristic peak located at 3339 cm^{-1} (corresponding to

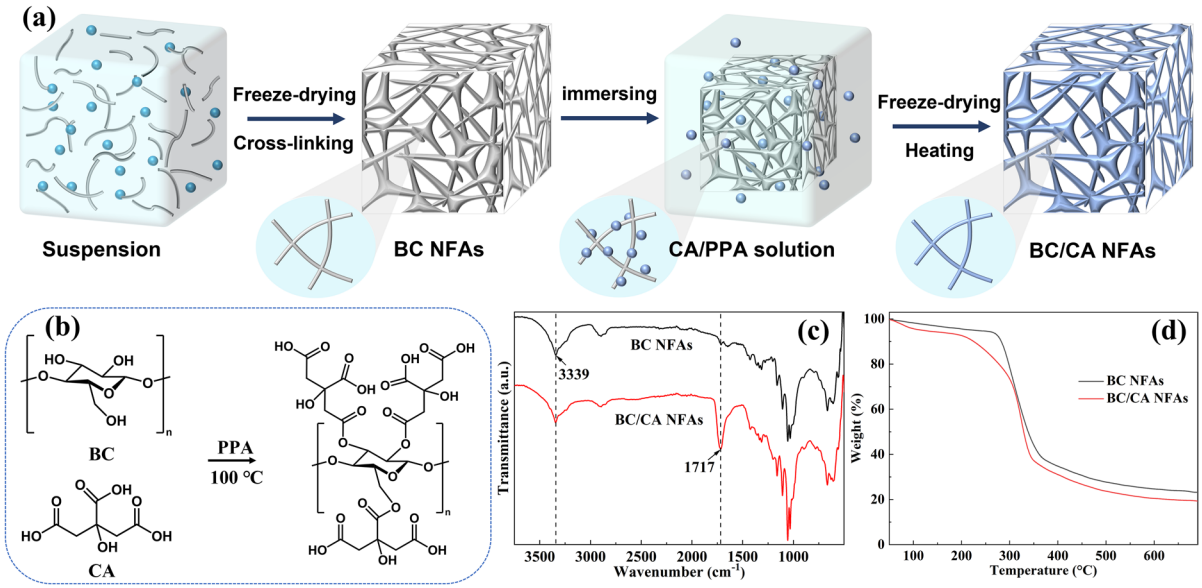

Fig. 1 **a** Schematic representation of preparation process of BC/CA NFAs, **b** schematic of grafting process of BC, **c** FTIR spectra of BC NFAs and BC/CA NFAs, **d** TGA curves of BC NFAs and BC/CA NFAs

-OH) decreased, and a new characteristic peak located at 1713 cm^{-1} (corresponding to C=O) appeared, demonstrating the reaction between BC nanofibers and CA (Fu et al. 2019a). The ester bond (O-C=O) located at 289.04 eV was observed in C 1 s spectrum of BC/CA NFAs (Fig. S6). BC/CA NFAs exhibited higher carboxyl content and lower oxygen to carbon atom ratio (Wang et al. 2023). The thermal degradation of BC nanofibers and BC/CA NFAs components was studied through TGA. The initial degradation temperature of BC nanofibers was about 270 °C, and around 7.9% residue remained, when the temperature reached 700 °C (Fig. S7). This is attributed to that the BC nanofibers could be carbonized to form carbon nanofibers under N_2 atmosphere (Li et al. 2020). The residual mass increased to 22.9%, after BC nanofibers were cross-linked to form aerogels (Fig. 1d). Besides the loss of water at 100 °C, only one degradation stage (between 269 and 370 °C) was observed in TGA curves of BC aerogels, which was attributed to the decomposition of BC. While, two separate degradation stages were found in TGA curves of BC/CA NFAs, in addition to the degradation of water. The first degradation stage occurred between 210 and 290 °C was attributed to the decomposition of grafted CA, indicating the lower thermal stability of carboxylate groups in BC/CA aerogels. The results were consistent with the previously reported literature (Chiou et al. 2013; Janusz et al. 2020). The second degradation stage was ascribed to the decomposition of BC. A weak broad signal was found in the range of 167–177 ppm (Fig. S8), confirming the presence of ester bonds and free carboxylic acid groups in BC/CA NFAs. The results of solid state 13C NMR analysis also demonstrated the successful grafting of CA (Spinella et al. 2016; Ghorpade et al. 2018).

Morphologies and structure of BC/CA NFAs

The SEM images of the BC NFAs were presented in Fig. 2a. BC NFAs exhibited highly interconnected open porous structure formed by pore walls during freeze-drying. Compared to BC NFAs, the morphology structure of BC/CA NFAs did not change significantly, only the pore size reduced (Fig. 2b), which was attributed to the formation of compact bonding structure among BC (Fu et al. 2016). The interconnected open porous of NFAs could provide abundant tortuous channels, allowing rapid penetration of protein solutions into aerogels (Wang et al. 2015). The high-resolution SEM images were employed to observe the BC pore walls. As shown in Fig. 2c, d, the pore walls in both BC NFAs and BC/CA NFAs were formed by the aggregation of BC nanofibers,

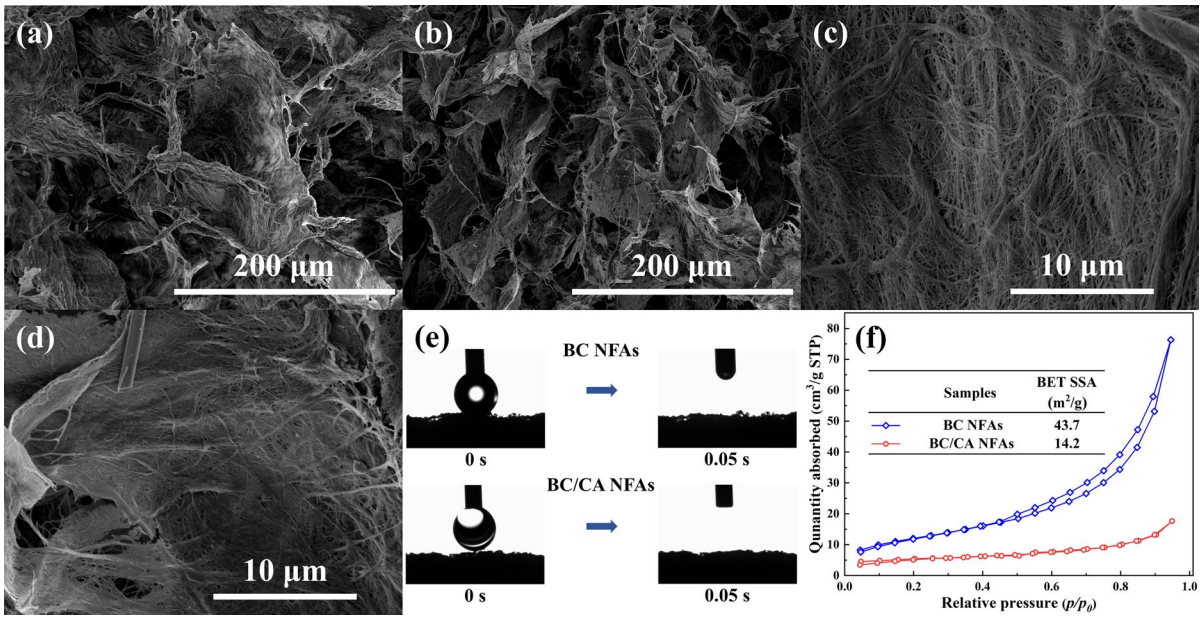

Fig. 2 SEM images of **a** BC NFAs and **b** BC/CA NFAs, high-resolution SEM images of **c** BC NFAs and **d** BC/CA NFAs, **e** photographs of dynamic measurements of water permeation on the surface of BC NFAs and BC/CA NFAs, **f** N_2 adsorption–desorption isotherms of BC NFAs and BC/CA NFAs

which was caused by cross-linking of glutaraldehyde (Qian et al. 2019). In contrast, the BC nanofibers were stacked and twined together, and could not generate pore wall structure (Fig. S9).

The surface wettability is a crucial factor affecting protein absorption performance of absorbents. Surface wettability of BC/CA NFAs was evaluated by water contact angle (WCA). As shown in Fig. 2e, once the water droplet touched the surface of NFAs, it was absorbed quickly. The WCA of both BC NFAs and BC/CA NFAs decreased to 0° in less than 1 s, confirming the good water wetting surface of aerogels. The hierarchical porous structure of BC/CA NFAs was studied by N_2 adsorption–desorption method. The absorption–desorption isotherms of aerogels before and after modification were exhibited in Fig. 2f. Type IV with a H3 hysteresis loop was observed in the curves, demonstrating NFAs possessed the typical mesoporous structure (Si et al. 2014; Li et al. 2015). The Brunauer–Emmett–Teller (BET) specific surface area of BC NFAs and BC/CA NFAs was 43.7 and 14.2 m^2/g, respectively. The decrease in BET specific surface area after grafting was attributed to the decrease in pore size. The BET specific surface area of prepared BC/CA NFAs is much higher than that of reported nanofiber-based chromatographic materials and commercial cellulose fibrous absorbents (Table S1) (Lv et al. 2017; Jiang et al. 2023; Ma et al. 2015; Dou et al. 2019; Yi et al. 2017). Therefore, the BC/CA NFAs fabricated in the work is suitable for practical protein absorption and separation process.

Mechanical properties of BC/CA NFAs

The BC nanofibers have been demonstrated to be efficient for the preparation of aerogels with good mechanical properties (Huang et al. 2022; Arabkhani and Asfaram 2020). The compression tests were carried out to evaluate the mechanical properties of BC/CA NFAs. The stress–strain curves ($\varepsilon = 60\%$) of BC NFAs with various glutaraldehyde contents were shown in Fig. S10. With increasing glutaraldehyde contents, the compressive stress of BC NFAs increased from 1.95 kPa to 3.64 kPa, indicating the introduction of glutaraldehyde improved mechanical properties. Figure 3a shows the stress–strain curves of BC NFAs and BC/CA NFAs. Two obvious distinct deformation regions were observed in these curves: a linear elastic deformation region at low strains

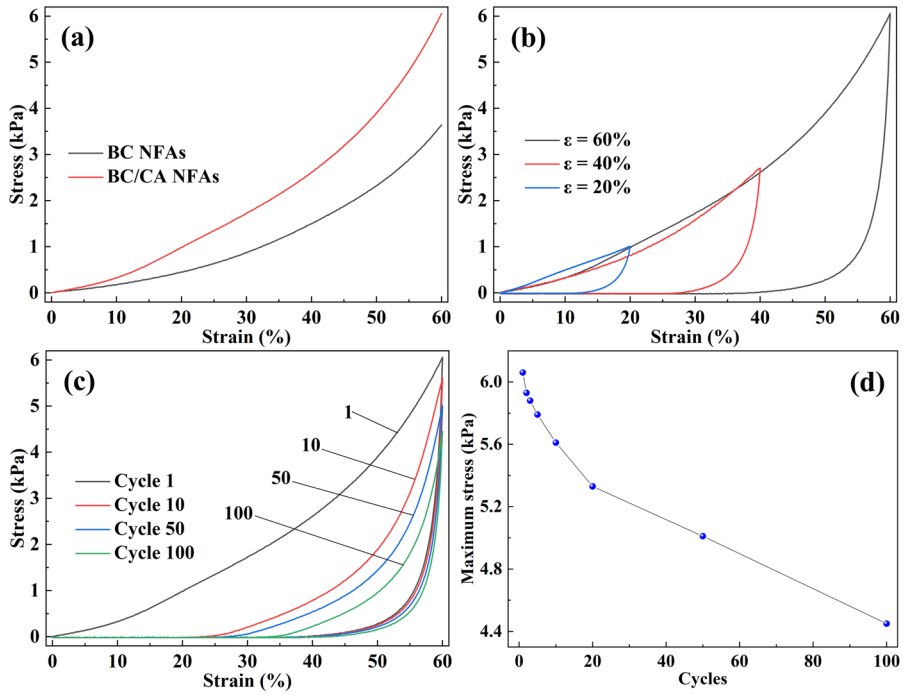

Fig. 3 **a** Compressive stress–strain curves (ε = 60%) of BC NFAs and BC/CA NFAs, **b** compressive stress–strain curves of BC/CA NFAs at different strain of 20%, 40% and 60%, **c** cyclic stress–strain curves of BC/CA NFAs at a strain of 60%, **d** the corresponding maximum stress

(ε < 20%) and a densification region at large strains (ε > 20%) (Lu et al. 2020). The maximum stress increased from 3.64 to 6.06 kPa at strain of 60%, after modification, demonstrating that the grafting of CA could enhance compressive strength. This is due to that the compact bonding structure among BC nanofibers formed during the processes of CA grafting could enhance the mechanical properties of NFAs (Fu et al. 2016). The compressive stress–strain curves of BC/CA NFAs at different strain of 20%, 40% and 60% are presented in Fig. 3b. The BC/CA NFAs exhibited good compressive properties, which were able to bear a large deformation without any collapse and recover to original shape after release of loading. It is obvious to observe a highly non-linear and hysteresis in those curves, which are typical viscoelastic and energy-dissipative behavior deformable materials (Lu et al. 2022). The compressive strain is 20%, 40%, and 60%, corresponding to the stress of 1.01, 2.71 and 6.06 kPa, respectively. The relatively high compressive strength is ascribed to robust mechanical properties of BC nanofibers and chemical crosslinking of glutaraldehyde.

The structural stability of BC/CA NFAs was evaluated to perform cyclic compression test. As shown in Fig. 3c, BC/CA NFAs were repeatedly compressed under a strain of 60% for 100 cycles. The hysteresis loops and a permanent deformation were found after cyclic compression, which was attributed to energy dissipation of aerogels during the repeated compression processes (Si et al. 2015). BC/CA NFAs could remain over 73% of the initial maximum stress after 100 cyclic compressions (Fig. 3d and Table S2), indicating the good compression fatigue resistance of BC/CA NFAs.

Optimization of protein absorption on BC/CA NFAs

As shown in Fig. 4a, the proteins were absorbed and immobilized on the surface of nanofibers through the electrostatic interaction. The carboxyl groups were grafted onto the BC nanofibers to endow them with surface electronegativity, which has been proved by zeta potential results (Fig. S11). Lysozyme was chosen as a positively charged protein template for protein absorption tests. The two new characteristic peaks (located at 1536 and 1648 cm^{-1}, respectively) in FTIR spectra of NFAs after absorption are attributed to amide groups of lysozyme (Fig. 4b), demonstrating the good lysozyme capture performance of BC/CA NFAs. As presented in Fig. 4c, the absorption capacity increased consistently with the increase of

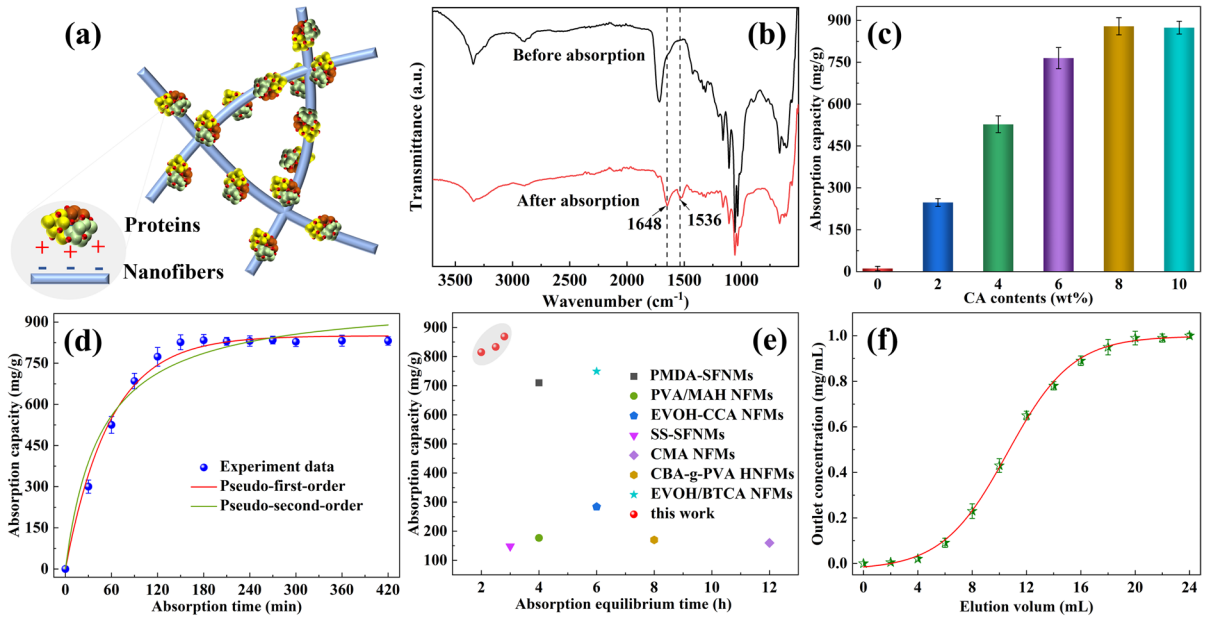

Fig. 4 **a** Schematic of absorption mechanism, **b** FTIR spectra of BC/CA NFAs before and after absorption, **c** absorption capacity of BC/CA NFAs with various CA contents, **d** the absorption capacity of BC/CA NFAs at different absorption time, **e** comparison of adsorption capacity and equilibrium time of reported absorbents, **f** lysozyme absorption breakthrough curves of BC/CA NFAs

CA contents, and the maximum absorption capacity of 868.9 mg/g was reached when the CA content was 8 wt%. With continued increase of CA contents, the absorption capacity remained constant. With increasing CA contents from 8 to 10 wt%, the ion-exchange capacity increased slightly (Fig. S12), illustrating the carboxyl groups on BC/CA NFAs had reached saturation. The absorption capacity of BC/CA NFAs was about 17 times higher than that of commercial Sartobind S and Sartobind C membranes adsorbents (Chiu et al. 2012).

The kinetic absorption performance is one of the most important factors affecting the actual absorption efficiency of absorbent materials (Amaly et al. 2020). The kinetic absorption performance of BC/CA NFAs was investigated by testing absorption capacity at varying adsorption time. As shown in Fig. 4d, it is clear that the absorption capacity increased sharply, then approached equilibrium value within 2.5 h, which was much shorter than these previously reported literatures (Yi et al. 2017; Dou et al. 2019). The pseudo-first-order, pseudo-second-order, Langmuir and Freundlich models are employed to investigate the type of interaction between lysozyme and BC/CA NFAs.

Pseudo-first-order models:

$$\ln(q_e - q_t) = -k_1 t + \ln q_e \tag{2}$$

Pseudo-second-order models:

$$\frac{t}{q_t} = \frac{1}{k_2 q_e^2} + \frac{t}{q_e} \tag{3}$$

Langmuir models:

$$\frac{1}{Q_e} = \frac{1}{Q_m} + \frac{1}{K_L Q_m C_e} \tag{4}$$

Freundlich models:

$$Q_e = K_F C_e^{1/n} \tag{5}$$

where q_t is the absorption amount at a given time, q_e is the absorption amount at equilibrium, t is the absorption time, k_1 and k_2 are the rate constants of the Pseudo-first-order and Pseudo-second-order models, Q_e and C_e are equilibrium absorption capacity and protein concentration at different initial concentration, respectively, Q_m is Langmuir adsorption capacity, K_L

and K_F are Langmuir and Freundlich adsorption constants, $1/n$ is the adsorption intensity constant.

The kinetic parameters of absorption process are listed in Table 1. The correlation coefficient (R^2) of pseudo-first-order model (0.99189) is higher than that of pseudo-second-order model (0.96638), indicating that the good match between absorption and pseudo-first-order model. The results demonstrated that the absorption of lysozyme on BC/CA NFAs is dependent on electrostatic interaction (Jiang et al. 2023). Moreover, the Langmuir and Freundlich models were introduced to study the lysozyme adsorption and capture process on BC/CA NFAs. As shown in Fig. S13 and Table S3, the R^2 of Langmuir models and Freundlich models is 0.98547 and 0.97722, respectively. Therefore, the absorption isotherms of BC/CA NFAs were fitted better with absorption process of Langmuir models.

Table 1 Kinetic parameters of absorption isotherm

Kinetic models	q_e (mg/g)	k	R^2
Pseudo-first-order models	850.11	0.02	0.99189
Pseudo-second-order models	987.34	2.20	0.96638

In comparison to most reported cellulose-based and carboxylated nanofibers-based protein absorbents (Qiao et al. 2022), BC/CA NFAs exhibited a higher absorption capacity and a shorter equilibrium time (Fig. 4e and Table S4), indicating the superior integrate application performance of BC/CA NFAs. The dynamic absorption performance was tested. The size-matched BC/CA NFAs (thickness of about 10 mm) were packed into columns to fabricate chromatography columns. The lysozyme solution was driven to penetrate chromatography columns solely by gravity. Figure 4f presents a typical lysozyme absorption breakthrough curve. The outlet concentration increased gradually and reached the initial lysozyme solution concentration. The calculated dynamic absorption was 655.35 mg/g, which was approximately 75% of the maximum static saturated absorption capacity. The good dynamic absorption performance of BC/CA NFAs is extremely important for their actual applications.

Absorption capacity on lysozyme at different pH values (3, 4, 5, 6, 7, 8, 9, 10 and 11) was detected to investigate the influence of protein solution on absorption performance. As shown in Fig. 5a, the absorption capacity exhibited a great dependence to the pH value. When the pH value of lysozyme

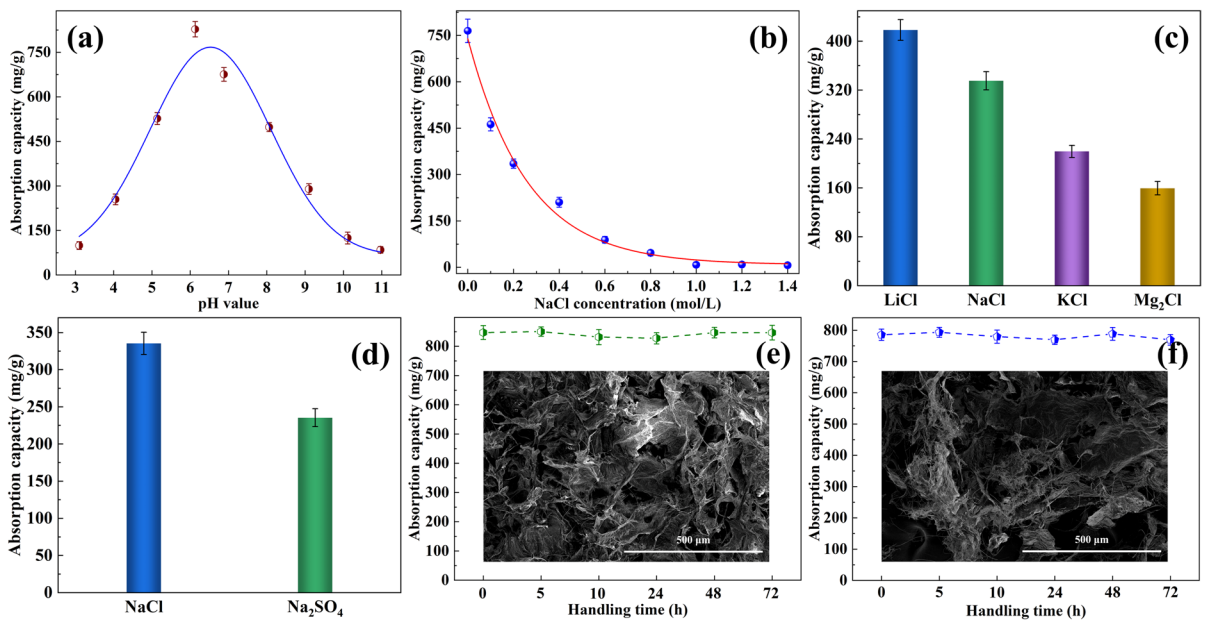

Fig. 5 Effect of **a** pH value, **b** ionic strength, **c** cationic species, **d** anionic species, **e** acid buffer and **f** alkaline buffer on absorption capacity of BC/CA NFAs (insets are the SEM images of BC/CA NFAs after acid/alkaline buffer treatment)

solution was about 2, the absorption capacity was relatively low. The maximum lysozyme absorption capacity was achieved with increasing pH value to about 6. which might be ascribed to increased ionized adsorption ligands with the increase of pH value (Li et al. 2015). The absorption capacity decreased sharply, with continued increase of pH value. This is due to that the positive charges of lysozyme reduced and even converted to negative charge at a relatively high pH value (Jiang et al. 2023), thus reducing the electrostatic interaction between BC/CA NFAs and lysozyme. Moreover, the neutral condition was beneficial to maintain the three-dimensional conformation and biological activity of protein. The following absorption experiments were carried out at pH value of about 6.

Lots of salt ions existed in the protein solution in the practical protein absorption applications. The NaCl was added into lysozyme solution to simulate the actual absorption. NaCl solutions with various concentration were used to regulate the ionic strength of lysozyme solutions. As presented in Fig. 5b, the absorption capacity decreased largely with increasing NaCl concentration, indicating that the absorption capacity was affected by the ionic strength (Fu et al. 2016). Therefore, the ionic strength in eluent can be regulated to realize protein elution. Beside ionic strength, the ionic species also possess important influences on the absorption capacity. The lysozyme absorption capacity in the presence of 0.2 M LiCl was much higher than that of in the presence of 0.2 M NaCl and KCl (Fig. 5c). The lysozyme absorption capacity in the presence of 0.2 M $MgCl_2$ is the lowest. This result proved that the larger radius and higher charges would result in lower absorption capacity. The anionic species also possess significant influences on the absorption capacity of BC/CA NFAs (Fig. 5d). The BC/CA NFAs were soaked into acid and alkaline buffer solution for a given time to evaluate acid and alkaline resistance. The absorption experimental results were presented in Fig. 5e, f, BC/CA NFAs still maintained a stable absorption capacity and micro-morphologies (insets of Fig. 5e, f) after being treated in acid and alkaline buffer for 72 h, highlighting their excellent structural stability.

Proteins with different surface charges under neutral conditions are selected to evaluate the selectively absorption of BA/CA NFAs. As displayed in Fig. 6a, BC/CA NFAs exhibited good absorption capacity to lysozyme, bromelain and papain. This is due to the electropositivity of the proteins under neutral conditions and can be absorbed by electronegative NFAs. While, the electronegative proteins (pepsin, ovalbumin and bull serum albumin) were barely absorbed. Therefore, BC/CA NFAs presented in this work can be used to separate electropositive and electronegative proteins. The absorbed BC/CA NFAs were eluted by 2 M NaCl solutions, then rinsed by deionized water for another absorption-elution cycle. As shown in Fig. 6b, the net absorption capacity of the regenerated BC/CA NFAs almost did not change after 10 cyclic processes, indicating the excellent cyclic

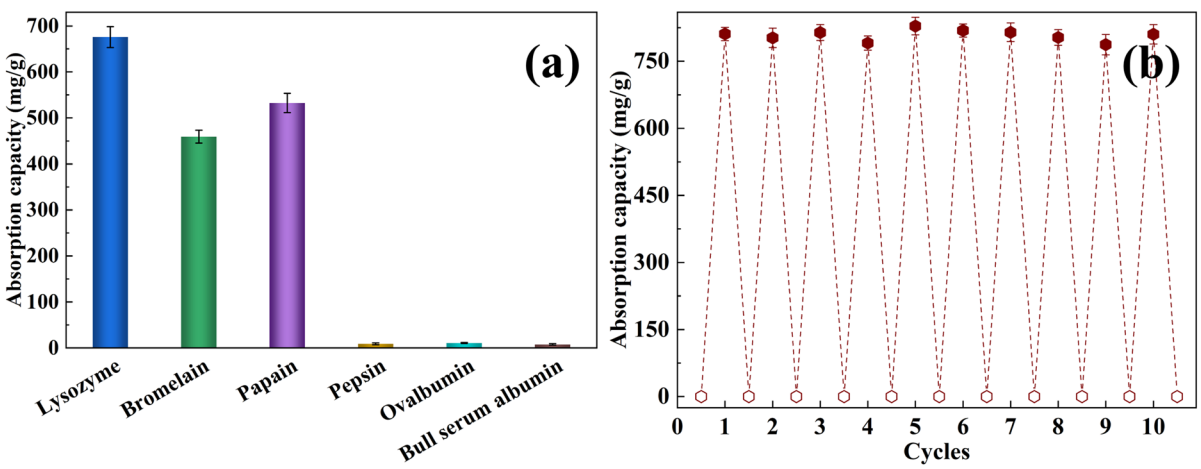

Fig. 6 **a** The absorption capacity to various proteins, **b** reusability of the BC/CA NFAs

performance of BC/CA NFAs. The good reusability of BC/CA NFAs mainly is ascribed to stability of tortuous porous fibrous structure and mechanical properties. Taking in account of favorable comprehensive properties, the BC-based protein absorbents represent a perfect candidate for next generation chromatographic media for highly efficient bio-separation.

Conclusion

We have reported that highly carboxylated nanofibrous aerogels (NFAs) could be constructed via graft of citric acid (CA) onto bacterial cellulose nanofibrous aerogels (BC NFAs). Successful grafting of CA was confirmed by FTIR, XPS, TGA, NMR and zeta potential results. Attributing to the cross-linking of glutaraldehyde and grafting of CA, the pore size and specific surface area of aerogels decreased, while the compressive strength increased. The obtained BC/CA aerogels were demonstrated to bind positively with the charged proteins through electrostatic interaction. With increasing CA contents, the lysozyme absorption capacity increased and achieved the maximum value of 868.9 mg/g within 2.5 h. The dynamic absorption capacity of 655.35 mg/g was reached solely under the drive of gravity. The absorption performance of BC/CA NFAs was sensitively affected by pH values, ionic strength and species, which weakened electrostatic interaction between aerogels and proteins. Furthermore, BC/CA NFAs exhibited excellent reusability, acid and alkali resistance, confirming their good stability of porous fibrous structure. We anticipate that the BC-based protein absorbents presented in this work offer a new option the design and development of chromatographic media in the fields of bio-separation and purification.

Acknowledgments Jiangsu University was acknowledged to provide characterization.

Author contributions JL conceptualized the work, analyzed data, and wrote the manuscript; YJ, ZW, ZL and YQ prepared bacterial cellulose nanofibrous aerogels and carried out protein absorption experiments; LG provided resources and guidance. All authors reviewed the manuscript.

Funding No funding.

Data availability All data generated or analyzed during this study are included in this published article.

Declarations

Conflict of interest The authors declare no competing interests.

Consent for publication All authors approved the final manuscript and the submission to this journal.

References

Amaly N, Ma Y, El-Moghazy AY, Sun G (2020) Copper complex formed with pyridine rings grafted on cellulose nanofibrous membranes for highly efficient lysozyme adsorption. Sep Purif Technol 250:117086

Arabkhani P, Asfaram A (2020) Development of a novel three-dimensional magnetic polymer aerogel as an efficient adsorbent for malachite green removal. J Hazard Mater 384:121394

Arbita AA, Paul NA, Cox J, Zhao J (2022) Amino acid sequence of two new milk-clotting proteases from the macroalga Gracilaria edulis. Int J Biol Macromol 211:499–505

Beaumont M, Jusner P, Gierlinger N, King AWT, Potthast A, Rojas OJ, Rosenau T (2021a) Unique reactivity of nanoporous cellulosic materials mediated by surface-confined water. Nat Commun 12(1):2513

Beaumont M, Nypelo T, Konig J, Zirbs R, Opietnik M, Potthast A, Rosenau T (2016) Synthesis of redispersible spherical cellulose II nanoparticles decorated with carboxylate groups. Green Chem 18(6):1465–1468

Beaumont M, Tardy BL, Reyes G, Koso TV, Schaubmayr E, Jusner P, King AWT, Dagastine RR, Potthast A, Rojas OJ, Rosenau T (2021b) Assembling native elementary cellulose nanofibrils via a reversible and regioselective surface functionalization. J Am Chem Soc 143(41):17040–17046

Chen H, Sharma SK, Sharma PR, Yeh HD, Johnson K, Hsiao BS (2019) Arsenic(III) removal by nanostructured dialdehyde cellulose-cysteine microscale and nanoscale fibers. ACS Omega 4(26):22008–22020

Cheng P, Liu K, Wan YC, Hu W, Ji CC, Huang P, Guo QH, Xu J, Cheng Q, Wang D (2022) Solution viscosity-mediated structural control of nanofibrous sponge for RNA separation and purification. Adv Funct Mater 32(20):2112023

Chiou BS, Jafri H, Cao T, Robertson GH, Gregorski KS, Imam SH, Glenn GM, Orts WJ (2013) Modification of wheat gluten with citric acid to produce superabsorbent materials. J Appl Polym Sci 129(6):3192–3197

Chiu HT, Lin JM, Cheng TH, Chou SY, Huang CC (2012) Direct purification of lysozyme from chicken egg white using weak acidic polyacrylonitrile nanofiber-based membranes. J Appl Polym Sci 125:E616–E621

Das R, Lindstrom T, Sharma PR, Chi K, Hsiao BS (2022) Nanocellulose for sustainable water purification. Chem Rev 122(9):8936–9031

Dou XY, Wang Q, Li ZL, Ju JP, Wang S, Hao LY, Sui KY, Xia YZ, Tan YQ (2019) Seaweed-derived electrospun nanofibrous membranes for ultrahigh protein adsorption. Adv Funct Mater 29(46):1905610

Ebrahimi A, Pazuki G, Mozaffarian M, Ahsaie FG, Abedini H (2023) Separation and purification of C-phycocyanin from *spirulina platensis* using aqueous two-phase systems based on triblock thermosensitive copolymers. Food Bioprocess Technol. https://doi.org/10.1007/s11947-023-03057-6

Fang K, Deng LG, Yin JY, Yang TH, Li JB, He W (2022) Recent advances in starch-based magnetic adsorbents for the removal of contaminants from wastewater: a review. Int J Biol Macromol 218:909–929

Fu QX, Duan C, Yan ZS, Si Y, Liu LF, Yu JY, Ding B (2018) Electrospun nanofibrous composite materials: a versatile platform for high efficiency protein adsorption and separation. Compos Commun 8:92–100

Fu QX, Liu LF, Si Y, Yu JY, Ding B (2019a) Shapeable, underwater superelastic, and highly phosphorylated nanofibrous aerogels for large-capacity and high-throughput protein separation. ACS Appl Mater Interfaces 11(47):44874–44885

Fu QX, Si Y, Duan C, Yan ZS, Liu LF, Yu JY, Ding B (2019b) Highly carboxylated, cellular structured, and underwater superelastic nanofibrous aerogels for efficient protein separation. Adv Funct Mater 29(13):1808234

Fu QX, Wang XQ, Si Y, Liu LF, Yu JY, Ding B (2016) Scalable fabrication of electrospun nanofibrous membranes functionalized with citric acid for high-performance protein adsorption. ACS Appl Mater Interfaces 8(18):11819–11829

Ge MY, Shen Y, Chen WM, Peng YT, Pan ZY (2019) Adsorption of bovine hemoglobin by sulfonated polystyrene nanospheres. ChemistrySelect 4(10):2874–2880

Ghorpade VS, Yadav AV, Dias RJ, Mali KK (2018) Fabrication of citric acid crosslinked -cyclodextrin/hydroxyethylcellulose hydrogel films for controlled delivery of poorly soluble drugs. J Appl Polym Sci 135(27):4652

Ghosh R (2002) Protein separation using membrane chromatography: opportunities and challenges. J Chromatogr A 952(1–2):13–27

He XM, Zhu GT, Lu W, Yuan BF, Wang H, Feng YQ (2015) Nickel(II)-immobilized sulfhydryl cotton fiber for selective binding and rapid separation of histidine-tagged proteins. J Chromatogr A 1405:188–192

Hu XD, Yang B, Hao M, Chen ZJ, Liu YB, Ramakrishna S, Wang XX, Yao JB (2023) Preparation of high elastic bacterial cellulose aerogel through thermochemical vapor deposition catalyzed by solid acid for oil-water separation. Carbohydr Polym 305:120538

Huang JY, Zhao M, Hao Y, Wei QF (2022) Recent advances in functional bacterial cellulose for wearable physical sensing applications. Adv Mater Technol 7(1):2100617

Jain P, Sun L, Dai JH, Baker GL, Bruening ML (2007) High-capacity purification of his-tagged proteins by affinity membranes containing functionalized polymer brushes. Biomacromol 8(10):3102–3107

Janusz W, Skwarek E, Sternik D, Pikus S, Pawlak D, Parus JL, Mikolajczak R (2020) Synthesis of yttrium citrate from yttrium carbonate hydroxide and citric acid. Mater Chem Phys 250:123113

Jiang Y, Lu J, Guo L (2023) Fabrication of highly carboxylated thermoplastic nanofibrous membranes for efficient absorption and separation of protein. Colloid Surf A 665:131203

Kluszczynska K, Peczek L, Rozanski A, Czernek L, Duchler M (2022) U6/miR-211 expression ratio as a purity parameter for HEK293 cell-derived exosomes. Acta Biochim Pol 69(2):409–415

Leitch ME, Li CK, Ikkala O, Mauter MS, Lowry GV (2016) Bacterial nanocellulose aerogel membranes: novel high-porosity materials for membrane distillation. Environ Sci Technol Lett 3(3):85–91

Li C, Ding YW, Hu BC, Wu ZY, Gao HL, Liang HW, Chen JF, Yu SH (2020) Temperature-invariant superelastic and fatigue resistant carbon nanofiber aerogels. Adv Mater 32(2):1904331

Li GT, Li TT, Li YL, An LB, Li W, Zhang ZM (2017) Preparation of pH-controllable nanofibrous membrane functionalized with lysine for selective adsorption of protein. Colloid Surf A 531:173–181

Li Y, Wen YA, Wang LH, He JX, Al-Deyab SS, El-Newehy M, Yu JY, Ding B (2015) Simultaneous visual detection and removal of lead(II) ions with pyromellitic dianhydride-grafted cellulose nanofibrous membranes. J Mater Chem A 3(35):18180–18189

Lu JW, Jiang YG, Xiao R, Jacob KI, Tao L, Li SJ, Guo L (2022) Chemical vapor deposition based superelastic and superhydrophoboic thermoplastic polymeric nanofibrous aerogels for water purification. J Inorg Organomet Poly 32(8):2975–2985

Lu JW, Li Y, Song W, Losego MD, Monikandan R, Jacob KI, Xiao R (2020) Atomic layer deposition onto thermoplastic polymeric nanofibrous aerogel templates for tailored surface properties. ACS Nano 14(7):7999–8011

Lu JW, Xu DD, Wei JK, Yan S, Xiao R (2017) Superoleophilic and flexible thermoplastic polymer nanofiber aerogels for removal of oils and organic solvents. ACS Appl Mater Interfaces 9(30):25533–25541

Lv H, Wang XQ, Fu QX, Si Y, Yin X, Li XR, Sun G, Yu JY, Ding B (2017) A versatile method for fabricating ion-exchange hydrogel nanofibrous membranes with superb biomolecule adsorption and separation properties. J Colloid Interface Sci 506:442–451

Ma JC, Wang XQ, Fu QX, Si Y, Yu JY, Ding B (2015) Highly carbonylated cellulose nanofibrous membranes utilizing maleic anhydride grafting for efficient lysozyme adsorption. ACS Appl Mater Interfaces 7(28):15658–15666

Ogata M, Sakamoto M, Yamauchi N, Nakazawa M, Koizumi A, Anazawa R, Kurumada K, Hidari KIPJ, Kono H (2022) Optimization of the conditions for the immobilization of glycopolypeptides on hydrophobic silica particulates and simple purification of lectin using glycopolypeptide-immobilized particulates. Carbohydr Res 519:108624

Orr V, Zhong LY, Moo-Young M, Chou CP (2013) Recent advances in bioprocessing application of membrane chromatography. Biotechnol Adv 31(4):450–465

Przybycien TM, Pujar NS, Steele LM (2004) Alternative bioseparation operations: life beyond packed-bed chromatography. Curr Opin Biotechnol 15(5):469–478

Qian LW, Yang MX, Chen HN, Xu Y, Zhang SF, Zhou QS, He B, Bai Y, Song WQ (2019) Preparation of a poly(ionic liquid)-functionalized cellulose aerogel and its application in protein enrichment and separation. Carbohydr Polym 218:154–162

Qiao LZ, Liao YX, Wang XW, Wang SS, Du KF (2022) Double-emulsion templated macroporous cellulose microspheres as a high-performance chromatographic media for protein separation. Cellulose 29(13):7263–7276

Rajesh S, Crandall C, Schneiderman S, Menkhaus TJ (2018) Cellulose-graft-polyethyleneamidoamine anion-exchange nanofiber membranes for simultaneous protein adsorption and virus filtration. ACS Appl Nano Mater 1(7):3321–3330

Sharma PR, Chattopadhyay A, Sharma SK, Hsiao BS (2017) Efficient removal of UO_2^{2+} from water using carboxycellulose nanofibers prepared by the nitro-oxidation method. Ind Eng Chem Res 56(46):13885–13893

Sharma PR, Sharma SK, Antoine R, Hsiao BS (2019) Efficient removal of arsenic using zinc oxide nanocrystal-decorated regenerated microfibrillated cellulose scaffolds. ACS Sustain Chem Eng 7(6):6140–6151

Sharma PR, Sharma SK, Lindstrom T, Hsiao BS (2020) Nanocellulose-enabled membranes for water purification: perspectives. Adv Sustain Syst 4(5):1900114

Si Y, Fu QX, Wang XQ, Zhu J, Yu JY, Sun G, Ding B (2015) Superelastic and superhydrophobic nanofiber-assembled cellular aerogels for effective separation of oil/water emulsions. ACS Nano 9(4):3791–3799

Si Y, Wang XQ, Li Y, Chen K, Wang JQ, Yu JY, Wang HJ, Ding B (2014) Optimized colorimetric sensor strip for mercury(II) assay using hierarchical nanostructured conjugated polymers. J Mater Chem A 2(3):645–652

Spinella S, Maiorana A, Qian Q, Dawson NJ, Hepworth V, McCallum SA, Ganesh M, Singer KD, Gross RA (2016) Concurrent cellulose hydrolysis and esterification to prepare a surface-modified cellulose nanocrystal decorated with carboxylic acid moieties. ACS Sustain Chem Eng 4(3):1538–1550

Wang FF, Zhang Y, Shi J, Sun L, Ullah A, Zhu CH, Kim IS (2023) Bioinspired and biodegradable functionalized graphene oxide/deacetylated cellulose acetate composite janus membranes for water evaporation-induced electricity generation. ACS Sustain Chem Eng 11(26):9792–9803

Wang P, Yin YK, Xu J, Chen SH, Wang H (2020) Facile synthesis of Cu^{2+}-immobilized imprinted cotton for the selective adsorption of bovine hemoglobin. Cellulose 27(2):867–877

Wang XL, Fu QX, Wang XQ, Si Y, Yu JY, Wang XL, Ding B (2015) In situ cross-linked and highly carboxylated poly(vinyl alcohol) nanofibrous membranes for efficient adsorption of proteins. J Mater Chem B 3(36):7281–7290

Yi SX, Dai FY, Ma Y, Yan TS, Si Y, Sun G (2017) Ultrafine silk-derived nanofibrous membranes exhibiting effective lysozyme adsorption. ACS Sustain Chem Eng 5(10):8777–8784

Yi SX, Dai FY, Wu YH, Zhao CY, Si Y, Sun G (2018) Scalable fabrication of sulfated silk fibroin nanofibrous membranes for efficient lipase adsorption and recovery. Int J Biol Macromol 111:738–745

Yu LL, Sun Y (2013) Protein adsorption to poly(ethylenimine)-modified Sepharose FF: II. Effect of ionic strength. J Chromatogr A 1305:85–93

Zhan CB, Li YX, Sharma PR, He HR, Sharma SK, Wang RF, Hsiao BS (2019) A study of TiO_2 nanocrystal growth and environmental remediation capability of TiO_2/CNC nanocomposites. RSC Adv 9(69):40565–40576

Zhang W, Zhang Y, Lu CH, Deng YL (2012) Aerogels from crosslinked cellulose nano/micro-fibrils and their fast shape recovery property in water. J Mater Chem 22(23):11642–11650

Zhang YD, Zhang LQ, Hu JN, Wang ZW, Meng DM, Li H, Zhou ZK, Yang R (2023) The structural characterization and color stabilization of the pigment protein-phycoerythrin glycosylated with oligochitosan. Food Hydrocolloid 136:108241

Zhao L, Wang H, Fu J, Wu X, Liang XY, Liu XY, Wu X, Cao LL, Xu ZY, Dong M (2022) Microfluidic-based exosome isolation and highly sensitive aptamer exosome membrane protein detection for lung cancer diagnosis. Biosens Bioelectron 214:114487